Photochemical & Photobiological Sciences

PAPER

View Article Online
View Journal | View Issue

Cite this: *Photochem. Photobiol. Sci.*, 2014, **13**, 660

A series of mononuclear lanthanide complexes featuring 3-D supramolecular networks: synthesis, characterization and luminescent properties for sensing guest molecules†

Waqar Ahmad, Lijuan Zhang* and Yunshan Zhou*

Received 4th October 2013,
Accepted 29th December 2013

DOI: 10.1039/c3pp50346a

www.rsc.org/pps

A new series of four isostructural mononuclear lanthanide complexes $Ln(HPDH)_3(H_2O)_3{\cdot}H_2O$ (Ln = Sm(III) **1**, Eu(III) **2**, Tb(III) **3** and Dy(III) **4**; H_2PDH = 6,7-dihydropyrido(2,3-*d*)pyridazine-5,8-dione) has been prepared and characterized by IR, elemental analysis, XRD and TG-DTA methods. Single crystal X-ray diffraction analysis of both complexes **1** and **3** revealed that the mononuclear discrete complexes form 3-D supramolecular networks *via* hydrogen bonds and offset stacking (–H···π) interactions. The photoluminescence study of the title complexes revealed the photoluminescent potential of the antenna ligand (H_2PDH) toward the concerned lanthanide cations. The luminescence based sensing ability of the partially dehydrated complex $Tb(HPDH)_3(H_2O)_3$ **3a** towards small solvent molecules, along with its reusability, has been studied. Isopropyl alcohol was found to be an excellent sensitizer, while tetrahydrofuran was a highly quenching solvent with a first order behavior towards the photoluminescence intensity. The photoluminescence intensity was found to decrease with the increase of the dielectric constant and normalized Dimroth–Reichardt E_T parameter values for protic solvents, while reverse behavior was observed for dipolar aprotic solvents.

1. Introduction

Photoluminescent Ln(III) complexes sensitized by organic ligands have excellent photophysical properties, such as distinctive sharp emissions, long excited-state luminescence lifetimes up to milliseconds and large stokes shifts, which make these complexes vital probes in sensing the guest molecules.[1] Luminescence based sensing and molecular recognition has become an essential tool for many biological processes in living cells and the environment.[2,3] So far, in the sensing mechanism the complexes are mainly thought to perform two functions: first they recognize the guest molecules (receptor) and then show a response by exhibiting a luminescence change either by quenching or enhancing (transducer). The luminescence intensity of a particular emission band can be used as a corresponding sensing signal which depends upon the tendency of host–guest interactions.[3] However, one has to admit that the details involved in the exact sensing mechanism of small guest molecules by luminescent complexes still remains ambiguous, as this ability of the complex is very sensitive to and dependent on various factors, such as the structural characteristics of the complex, nature of the ligand,[1b,c] coordination environment of the metal,[1d] nature of the pore surfaces,[4] and their interactions with guest species through coordination bonds, π···π interactions and hydrogen bonding *etc.*,[5] which have provided the solid ground to develop luminescent sensing complexes. Further the luminescent properties of Ln(III) cations are largely influenced by the radiationless deactivation process that occurs upon interaction with OH, NH, and CH oscillators of the solvent molecules, which can simply be reduced by the entire filling of the first coordination sphere.[6] Although water molecules in the first coordination sphere usually quench the luminescence of a lanthanide cation, at the same time they offer chances to be replaced by other organic solvent molecules when such complexes are immersed in organic solvents and consequently help in sensitizing the lanthanide cation.

Lanthanide based metal–organic frameworks (LnOFs) have been extensively studied for guest sensing.[1,7] However, to the best of our knowledge, mononuclear discrete lanthanide

State Key Laboratory of Chemical Resource Engineering, Institute of Science, Beijing University of Chemical Technology, Beijing 100029, P. R. China.
E-mail: ljzhang@mail.buct.edu.cn, zhouys@mail.buct.edu.cn

†Electronic supplementary information (ESI) available: ^1H NMR spectrum of ligand H_2PDH, IR spectra of ligand and titled complexes, selected hydrogen bondings of complex **1**, nonradiative deactivation mechanism, reusability of the complex **3a** (Fig. S1 to S5) and crystal data of complex **1** and **3**, selected bond lengths and bond angles and hydrogen bonding interactions in complex **1** (Tables S1 to S3). CCDC 960629 and 960631. For ESI and crystallographic data in CIF or other electronic format see DOI: 10.1039/c3pp50346a

complexes have rarely been studied for guest sensing.[8] It is a well known fact that relatively weak interactions have been extensively utilized for molecular recognition associated with biological activity, and for crystal engineering of molecular solids.[9] Such non-coordinated synergistic interactions are more flexible than coordination bonds, and have an additional influence on the structure and luminescence properties of complexes.[10] Therefore, it is expected that mononuclear discrete lanthanide complexes, which can normally construct 3-D networks by hydrogen bonds and/or offset stacking (–H···π) as well as other supramolecular interactions, may show distinct luminescence properties for sensing guest molecules.

Herein, we selected a stable, conjugated and rigid ligand [6,7-dihydropyrido(2,3-*d*)pyridazine-5,8-dione (H_2PDH)], having different coordination atoms (N– and O–), assuming it as an attractive candidate for antenna sensitization, and created a new series of four isostructural mononuclear lanthanide complexes $Ln(HPDH)_3(H_2O)_3{\cdot}H_2O$ (Ln = Sm(III) **1**, Eu(III) **2**, Tb(III) **3**, Dy(III) **4**), which feature hydrogen-bonded 3-D networks. The photoluminescence properties of the complexes, selective sensing and reproducing ability of the partially dehydrated complex $Tb(HPDH)_3(H_2O)_3$ **3a** with respect to the dielectric constant, coordination ability and Reichardt's solvent polarity parameters values of solvents are investigated.

2. Experimental

2.1. Reagents and general techniques

All chemicals were obtained from commercial sources, of reagent grade quality and used without further purification. IR (KBr pellets) spectra were recorded on a Nicolet FT IR-170SX spectrometer in the 4000–400 cm^{-1} range. Elemental analyses for C, H, N were performed on a Perkin-Elmer 240C analytical instrument, while analyses for Eu, Tb, Sm and Dy were performed using an ICPS-7500 model inductively coupled plasma emission spectrometer (ICP-ES) with all samples dissolved in dilute hydrochloric acid. Thermogravimetric analyses (TGA) and differential thermal analyses (DTA) were performed on a NETZSCH STA 449C unit at a heating rate of 10 °C min^{-1} under a nitrogen atmosphere. Powder X-ray diffraction (XRD) measurements were performed on a Rigaku-Dmax 2500 diffractometer at a scanning rate of 15° min^{-1} in the 2θ range from 5° to 90° with graphite monochromatized Cu Kα radiation (λ = 0.15405 nm). Photoluminescence measurements of all complexes (solids and emulsions) were recorded using a Hitachi F-7000 FL spectrofluorometer with both excitation and emission slits of 5 nm, using a xenon arc lamp as the light source (150 W), the photomultiplier tube voltage was 400 V, the scan speed was 1200 nm min^{-1} and a 350 nm filter was also used. The luminescence decay curves were obtained with an Edinburgh spectrometer FLS980 using a tunable laser with a 262.8 nm wavelength, bandwidth of 10.2 nm, pulse width of 930.8 ps and a gate of 100 ns. Single-crystal X-ray diffraction data was collected on a Bruker APEX2 X-Diffraction instrument with Mo Kα radiation (λ = 0.71073 Å) in the ω scan mode. The structure was solved by a direct method and refined anisotropically using a full-matrix least-squares method with the SHELX 97 program package.[11] The non-hydrogen atoms were located in successive difference Fourier syntheses. The final refinement was performed by full matrix least squares methods with anisotropic thermal parameters for non-hydrogen atoms on $|F|^2$.[12]

2.2. Hydrothermal synthesis of 6,7-dihydropyrido(2,3-*d*)-pyridazine-5,8-dione (H_2PDH)

The 2,3-pyridinedicarboxylic acid chloride was prepared according to the literature,[13] except that we used toluene at the place of more toxic benzene, as a result the reaction took one hour longer than the reported method. The as-prepared 2,3-pyridinedicarboxylic acid chloride was immediately used without further purification. A mixture of 2,3-pyridinedicarboxylic acid chloride 10.2 g (0.05 mol) and hydrazine dihydrochloride 5.25 g (0.05 mol) were dispersed in 60 mL of distilled water, which was then transferred to a 80 mL Teflon-lined autoclave and maintained at 170 °C for 24 h then cooled slowly to room temperature (Scheme 1).

The obtained off-white needle crystals were collected and repeatedly washed with distilled water followed by absolute ethanol, and then dried at room temperature naturally (yield: 5.6 g; 55.5% based on 2,3-pyridinedicarboxylic acid chloride). Anal. calcd for $C_7H_5N_3O_2$ (H_2PDH): C, 51.53; H, 3.06; N, 25.76. Found: C, 52.04; H, 3.09; N, 25.18; ^{1}HNMR (400 MHZ, D_2O): δ 9.1 (d, J = 4, 1H), δ 8.92 (d, J = 8, 1H), δ 8.79 (dd, J = 8, 1H), δ 8.17 (dd, J = 2, 6, 1H), δ 8.05 (dd, J = 4, 8 1H) (Fig. S1, ESI†). IR (KBr, cm^{-1}) (Fig. S2†): 3477 (s), 3186 (s), 3108 (s), 3046 (s), 2928 (s), 1697 (s), 1641 (m), 1585 (m), 1501 (s), 1453 (s), 1405 (s), 1349 (s), 1217 (s), 1092 (s), 842 (s), 792 (s), 710 (s), 646 (s).[14]

2.3. Hydrothermal synthesis of $Sm(HPDH)_3(H_2O)_3{\cdot}H_2O$ (1)

The pale yellow bold needle crystals of complex **1** were obtained by a simple hydrothermal reaction of Sm_2O_3 (0.043 g, 0.12 mmol) and H_2PDH (0.065 g, 0.4 mmol) in a 10 mL aqueous solution at 170 °C for 4 days in 25 mL Teflon-lined autoclave. Yield: *ca.* 0.0127 g (29.7% based on Sm). Anal. calcd for $C_{21}H_{20}N_9O_{10}Sm$: C, 35.58, H, 2.82, N, 17.78. Found: C, 34.86, H, 2.27, N, 17.39%. IR (KBr, cm^{-1}) (Fig. S2†): 1634 (s), 1495 (s), 1371(s), 1084 (s), 1014 (s), 814 (m), 752 (s).

2.4. Hydrothermal synthesis of $Eu(HPDH)_3(H_2O)_3{\cdot}H_2O$ (2)

The colorless needle crystals of complex **2** were obtained by a simple hydrothermal reaction of Eu_2O_3 (0.042 g, 0.12 mmol) and H_2PDH (0.065 g, 0.4 mmol) in a 10 mL aqueous solution

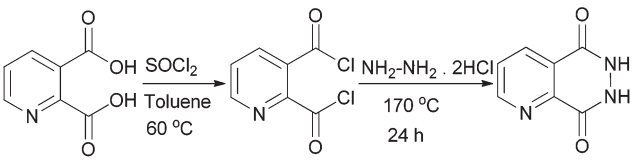

Scheme 1 Synthesis of ligand H_2PDH.

at 170 °C for 4 days. Yield: *ca.* 0.0124 g (29.7% based on Eu). Anal. calcd for $C_{21}H_{20}N_9O_{10}Eu$: C, 35.50, H, 2.82, N, 17.75. Found: C, 35.05, H, 2.39, N, 17.01%. IR (KBr, cm^{-1}) (Fig. S2†): 1632 (s), 1405 (s), and 1101 (w).

2.5. Hydrothermal synthesis of $Tb(HPDH)_3(H_2O)_3{\cdot}H_2O$ (3)

The light yellow needle crystals of complex **3** were obtained by a similar hydrothermal method to that of complex **1** except with the use of Tb_4O_7 (0.046 g, 0.062 mmol). Yield: *ca.* 0.0138 g (30.1% based on Tb). Anal. Calcd $C_{21}H_{20}N_9O_{10}Tb$: C, 35.16, H, 2.79, N, 17.57. Found: C, 34.86, H, 2.26, N, 17.19%. IR (KBr, cm^{-1}) (Fig. S2†): 1635 (s), 1495(w), 1383 (s), 1028 (s).

2.6. Hydrothermal synthesis of $Dy(HPDH)_3(H_2O)_3{\cdot}H_2O$ (4)

The light yellow needle crystals of complex **4** were obtained by a simple hydrothermal reaction of Dy_2O_3 (0.046 g, 0.12 mmol), and H_2PDH (0.065 g, 0.4 mmol) in a 10 mL aqueous solution at 170 °C for 4 days. Yield: *ca.* 0.0143 g (31.3% based on Dy). Anal. calcd for $C_{21}H_{20}N_9O_{10}Dy$: C, 34.98, H, 2.77, N, 17.49. Found: C, 34.47, H, 2.42, N, 17.18%. IR (KBr, cm^{-1}) (Fig. S2†): 1648 (s), 1495 (s), 1480 (w), 1377 (s), 1036 (s).

2.7. Partial dehydration of complexes 1–4

Complexes **1–4** were heated at 150 °C overnight to remove one uncoordinated water, to yield partially dehydrated phase complexes as **1a–4a**. Elemental analyses of the partially dehydrated complexes show that the percentages of C as 36.51, 36.40, 36.02, 36. 84, of H as 2.59, 2.58, 2.56, 2.55 and of N as 18.24, 18.19, 18.01, 17.80 for complexes **1a–4a**, respectively, which are in good agreement with the elemental compositions of $C_{21}H_{18}N_9O_9Ln$ (where Ln = Sm for complex **1a**, Eu for complex **2a**, Tb for complex **3a** and Dy for complex **4a**).[15]

3. Results and discussion

3.1. Synthesis

The synthesis of the H_2PDH ligand has been carried out in an easy fashion by the treatment of aromatic diacidchloride with hydrazine dihydrochloride (1 : 1) in water by a hydrothermal method at 170 °C for 24 h and achieved a reasonable yield of 55.5% (Scheme 1). The reactions between the lanthanide oxides and H_2PDH under hydrothermal conditions resulted in the formation of four new lanthanide complexes **1–4**. Under the defined optimal conditions (the molar ratio of Ln(III)/H_2PDH = 1 : 4, reaction temperature = 170 °C, reaction time = 4 days, 25 mL Teflon-lined autoclave), almost a 25% yield of all complexes were obtained.

3.2. IR

The IR spectrum of free ligand H_2PDH shows a strong absorption band at 1697 cm^{-1}, which may be assigned to the stretching vibration of the carbonyl group υ(C═O).[16] The medium intensity bands appearing at 3352 and 3384 cm^{-1} can be assigned to the aromatic υ(N–H) stretching, and the peaks at 848 and 786 cm^{-1} are assigned to the aromatic C–H bonds.[17] The bands in the region of 1595–1501 cm^{-1} are attributed to aromatic υ(C═N) and υ(C═C).[18] The IR spectra of complexes **1–4** are very similar, the characteristic frequency of the free ligand υ(C═O) at 1697 cm^{-1} shifts to 1634, 1632, 1635 and 1648 cm^{-1} for complexes **1** to **4** respectively, indicating that the oxygen atom of the carbonyl group of the ligand is involved in the coordination interaction with Ln(III) in the four complexes, as shown in Fig. S2.†

3.3. XRD

The purity of the title complexes was confirmed by X-ray powder diffraction analysis, in which the experimental spectra of complex **1** (Fig. 1b), complex **2** (Fig. 1c), complex **3** (Fig. 1d) and complex **4** (Fig. 1e) are almost consistent with the simulated spectra XRD pattern (Fig. 1a) generated on the basis of structural data of the crystal for the complex **1**. Based on the powder XRD patterns, complexes **1–4** are isostructural, no other peaks can be found in the pattern of the four complexes, revealing that there is no impurity in the products.

3.4. Structural description of the $Ln(HPDH)_3(H_2O)_3{\cdot}H_2O$ complexes

As all of the complexes were isostructural, for representation only complex **1** is selected as a model for structural description. A summary of the crystallographic data and structural determination parameters of complexes **1** and **3** are given in Table S1.† CIF files for the structures reported in this paper have been provided and the deposition numbers are given in Table S1.†

Complex **1** crystallizes in the monoclinic crystal system and belongs to the $P2_1/c$ space group. Single crystal X-ray analysis revealed that the asymmetric unit is composed of one Sm(III) center, three $HPDH^-$ ligands, three coordinated water molecules (OW7, OW8 and OW9) and one uncoordinated water

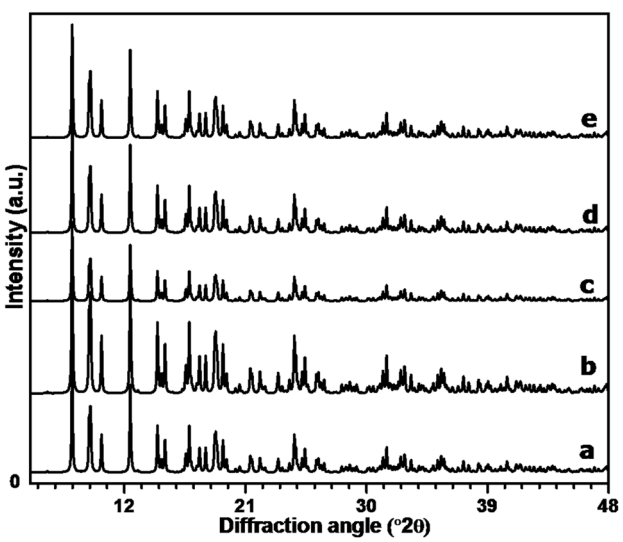

Fig. 1 X-Ray powder diffraction (XRD) analysis patterns of complex **1** simulated (a), experimental (b), complexes **2** (c), **3** (d) and **4** (e).

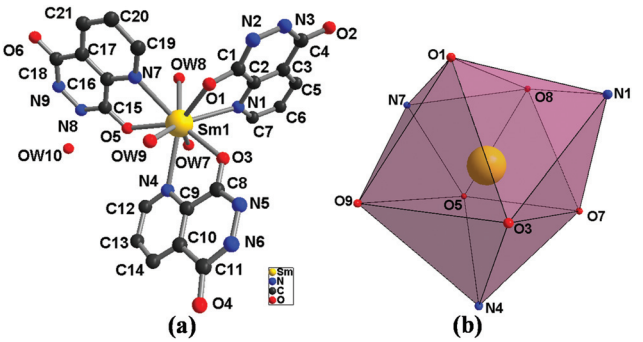

Fig. 2 The coordination environment around Sm(III) in complex **1** with labeling scheme (all hydrogen atoms are omitted for clarity) (a), and coordination polyhedra for the one central Sm(III) ion (b). Color code: yellow, Sm; blue, N; red, O; black, C.

molecule (OW10) (Fig. 2a). Fig. 2b reveals that each independent Sm(III) center is nine coordinated with the coordination geometry of a distorted tricapped trigonal prism, which is enclosed by three acylamino oxygen atoms (O1, O3 and O5), three pyridyl nitrogen atoms (N1, N4 and N7) from three different $HPDH^-$ ligand molecules, and three coordinated water oxygen atoms (OW7, OW8 and OW9).

The six Sm1–O distances (from the three coordinated water molecules and from the three different pyrazine rings of $HPDH^-$ ligands), Sm1–OW7 = 2.4017(3) Å, Sm1–OW8 = 2.4549 (4) Å, Sm1–OW9 = 2.5680(3) Å, Sm1–O1 = 2.3519(2) Å, Sm1–O3 = 2.3855(3) Å, and Sm1–O5 = 2.4044(3) Å are almost equivalent to each other. Similarly, the three Sm1–$N_{pyridyl}$ distances, 2.6958(3) Å for N1, 2.7412(5) Å for N4 and 2.6340(3) Å for N7 are also comparable with each other. The bond lengths of Sm1–OW9 and Sm1–N4 are the larger bond lengths among all the Sm1–O and Sm1–N bonds in complex **1**. The O–Sm1–O and O–Sm1–N bond angles vary from 76.18° to 139.57° and 62.73° to 145.16°, respectively (Table S2†).

Each $HPDH^-$ molecule adopts a uni-connected coordination mode, the pyridyl N atom (N1/N4/N7) and one acylamino O atom (O1/O3/O5) chelate to one Sm(III) center while other acylamino O atoms (O2/O4/O6) and pyrazine N atoms (N2/N3, N5/N6, N8/N9) remain uncoordinated.

The mono nuclear discrete units form a 1D chain along the *b* direction (top right in Fig. 3) through hydrogen bonding interactions (OW8···O4 = 2.707(3) Å). The 1D chains further interact with lattice water molecules OW10 *via* hydrogen bonding interactions (OW9···OW10 = 3.012(4) Å), and then form 2D layers (top right in Fig. 3) by offset stacking interactions of the H10a of the lattice water molecules OW10 in a chain and the pyridyl ring (C2, C3, C5–C7, and N1) (OW10–H10a···π = 2.689 Å) of its neighbouring chain (top left in Fig. 3) (Table S3†).

Interestingly, the 2D layers further form a 3D structure *via* complex supramolecular interactions (bottom right in Fig. 3). Detailed hydrogen bonding interactions between adjacent 2D layers (Fig. S3†) are shown in Table S3,† which are in the range of 2.853(4) Å–3.130(4) Å. Further scrutiny of the X-ray structure of complex **1** highlights the existence of more O/N/C–H···π (offset stacking) interactions[19] between the adjacent 2D layers. There are four inter 2D layer offset stacking interactions as follows (bottom left in Fig. 3): N6–H6 of pyrazinedione ring (C8–C11, N5 and N6) of a 2D layer interacting with the pyridyl ring (C9, C10, C12–C14, and N4) (N6–H6···π = 3.262 Å) of a neighboring 2D layer; C12–H12 of the pyridyl ring (C9, C10, C12–C14, and N4) of a 2D layer with the pyrazinedione ring (C8–C11, N5 and N6) (C12–H12···π = 3.412 Å) of a neighbouring 2D layer; C6–H6A of pyridyl ring (C2, C3, C5–C7, and N1) of a 2D layer interacting with pyrazinedione ring (C1–C4, N2 and N3) (C6–H6A···π = 3.758 Å) of a neighboring 2D layer; N3–H3 of pyrazinedione ring (C1–C4, N2 and N3) of a 2D layer interacting with the pyridyl ring (C2, C3, C5–C7, and N1) (N3–H3···π = 3.44 Å) of a neighboring 2D layer.

The distances between the adjacent Sm···Sm within a 1D chain is *ca.* 9.3 Å, while the adjacent 1D chains lie at a distance of 10.9 Å in the *c* direction and adjacent parallel 2D layers are *ca.* 6.0 Å far away from each other (based on Sm···Sm).

3.5. Photoluminescent properties

The excitation bands for complex **1** under the emission of 561 nm show three main peaks at 226, 271 and 333 nm. Under the excitation of 271 nm (the maximum excitation wavelength), complex **1** shows three emission peaks at 562, 590 and 670, which may be attributed to the $^4G_{5/2} \rightarrow {}^6H_{5/2}$, $^4G_{5/2} \rightarrow {}^6H_{7/2}$, $^4G_{5/2} \rightarrow {}^6H_{9/2}$ transitions, respectively.[20] Further, when the partially dehydrated complex **1a** was submitted for evaluation of the photoluminescence properties under the same conditions, it was found that the PL (excitation and emission) intensity was enhanced two fold as compared to complex **1** (Fig. 4).

Complex **2** emits characteristic red luminescence from the Eu(III) ion in the solid state under UV light irradiation, and the corresponding excitation and emission spectra of complex **2** and complex **2a** are shown in Fig. 5.

The strong broad centered band at 270 nm in the excitation spectrum of complex **2** is ascribed to the electronic transitions of the H_2PDH ligand. The peaks at 390, 464 and 535 nm can be assigned to the $^7F_0 \rightarrow {}^5L_6$, $^7F_0 \rightarrow {}^5D_2$ and $^7F_0 \rightarrow {}^5D_1$ transitions of the Eu(III) ion, respectively (Fig. 5). The detection of the band (centered at 270 nm) together with its higher intensity relatively to the intra-$4f^N$ transitions, points out more efficient luminescence sensitization *via* the ligands excited states than the direct intra-$4f^N$ excitation.[21]

The room temperature emission spectra (Fig. 5) of complex **2** in the solid state, excited at 270 nm (the maximum excitation wavelength), shows sensitized luminescence bands that correspond to the typical Eu(III) $^5D_0 \rightarrow {}^7F_n$ (n = 1, 2, 3, 4) transitions. Complex **2** shows intense red luminescence and the strong intensities of a magnetic dipole emission at 592 nm and hypersensitive induced electric dipole emission at 615 nm, which are attributed to $^5D_0 \rightarrow {}^7F_1$ and $^5D_0 \rightarrow {}^7F_2$ transitions, respectively.[22] The magnetic dipole emission of the $^5D_0 \rightarrow {}^7F_1$ transition is relatively weaker and largely independent of the coordination sphere, *i.e.*, the ligand field.[23] The electric dipole $^5D_0 \rightarrow {}^7F_2$ transition centered at 615 nm is extremely sensitive

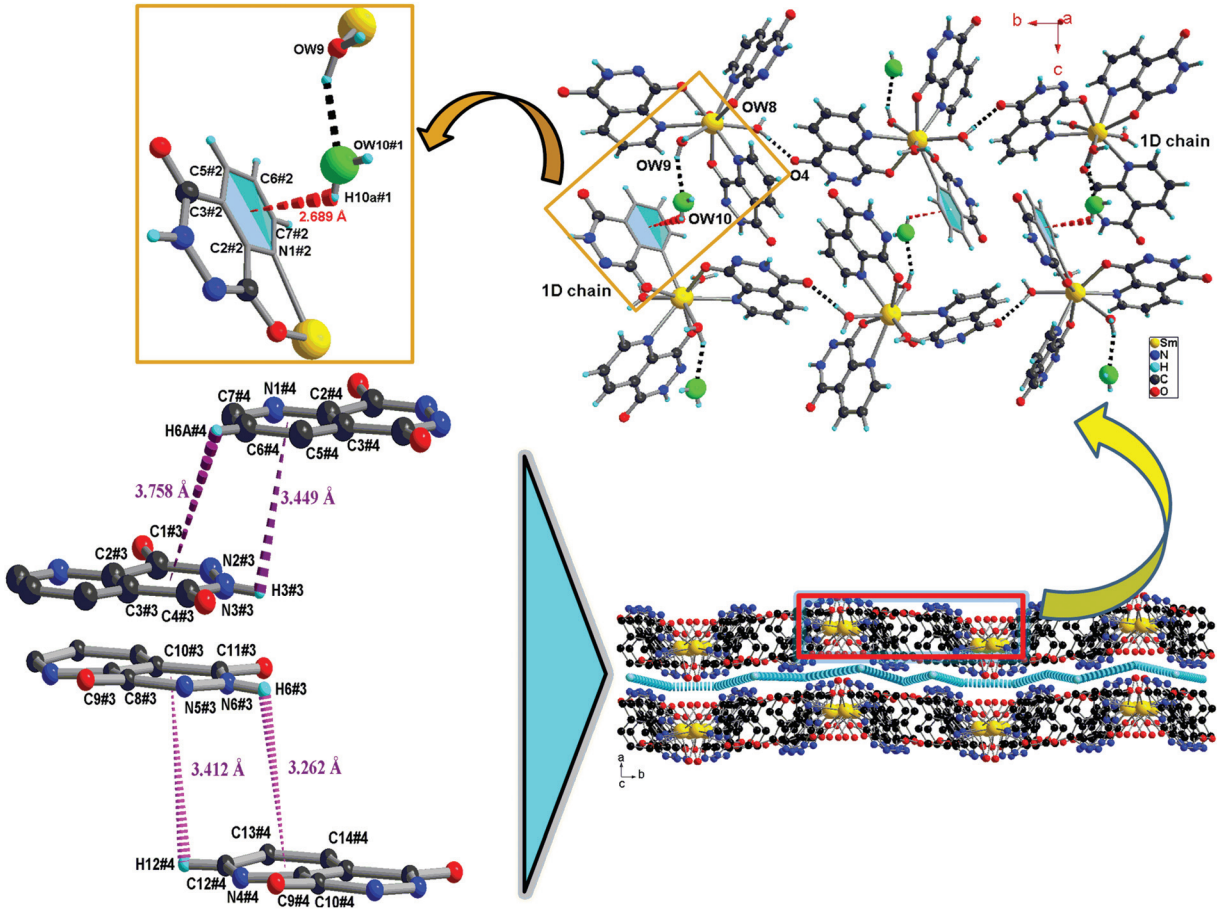

Fig. 3 The schematic representation of the formation of the 3D supramolecular network (bottom right) from 2D layers (top right) composed of 1D chains in complex **1**. The hydrogen bonds (OW8···O4) responsible for the formation of the 1D chains are represented by black dotted lines; the hydrogen bonds (OW9···OW10) and the OW10–H···π interactions responsible for the formation of the 2D layers from the 1D chains are highlighted (top left) in ball-and-stick model; the interactions (N6–H6···π, C12–H12···π and C6–H6···π, N3–H3···π), which are responsible for the formation of the 3D supramolecular structure from the 2D layers, are highlighted in the ball-and-stick model (bottom left). The hydrogen bonds existing in between the 2D layers are not shown for clarity. Symmetry code: #1 = –*x*, 1/2 + *y*, 1/2 – *z*, #2 = 1 – *x*, 1 – *y*, –*z*, #3 = 1 – *x*, –1/2 + *y*, –1/2 – *z* #4 = –*x*, –1/2 + *y*, –1/2 – *z*. Inter 2D layer hydrogen bonds are omitted for clarity. The bright green balls are oxygen atoms of uncoordinated water molecules, H atoms are shown in cyan, and the color codes for the other atoms are the same as in Fig. 2.

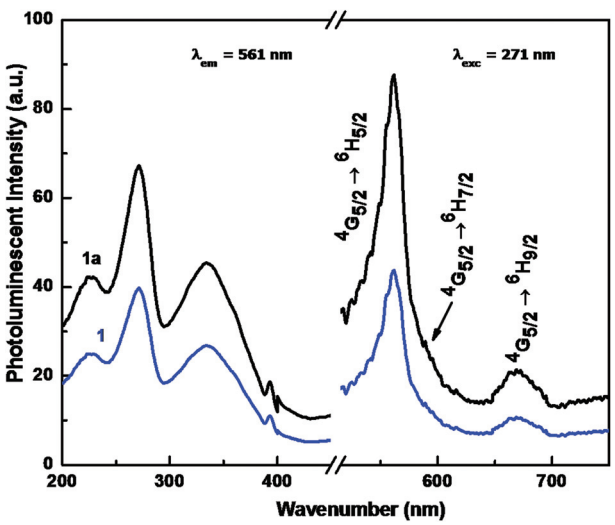

Fig. 4 Excitation and emission spectra of $Sm(HPDH)_3(H_2O)_3{\cdot}H_2O$ **1** (blue) and $Sm(HPDH)_3(H_2O)_3$ **1a** (black) at λ_{em} = 561 nm and λ_{exc} = 271 nm.

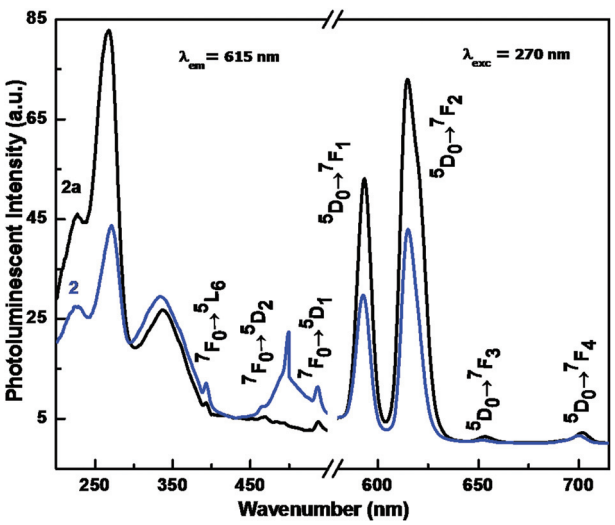

Fig. 5 Excitation and emission spectra of $Eu(HPDH)_3(H_2O)_3{\cdot}H_2O$ **2** (blue) and $Eu(HPDH)_3(H_2O)_3$ **2a** (black) at λ_{em} = 615 nm and λ_{exc} = 270 nm.

to the symmetry of the coordination sphere.[24] The intensity ratio of the $^5D_0 \rightarrow {}^7F_2/{}^5D_0 \rightarrow {}^7F_1$ transition is 1.40, indicating that the Eu^{3+} ion has an almost symmetrical coordination sphere,[25,26] which is consistent with the single crystal structure results.

The distortion of the symmetry around the metal ion causes an intensity enhancement of the electric dipole transitions, such as the hypersensitive $^5D_0 \rightarrow {}^7F_2$ transition (Fig. 5). Two emission peaks with weak intensities of the induced electric dipole emission at 653 nm and 702 nm correspond to the $^5D_0 \rightarrow {}^7F_3$ and $^5D_0 \rightarrow {}^7F_4$ transitions, respectively.[27] When the partially dehydrated complex **2a** was submitted for luminescence, it shows all the characteristic peaks similar to complex **2**, while the intensities of both the excitation and emission spectra are increased two fold as compared to complex **2** (Fig. 5).

The room temperature excitation bands of complex **3** under an emission wavelength of 546 nm possesses three main peaks at 230 and 268 nm and one detectable small band at 302 nm, which may be attributed to the $^7F_6 \rightarrow {}^5D_0$ transition as an intra-configurational forbidden $^4F_8 \rightarrow {}^4F_8$ transition of the Tb(III) ion.[28] The appearance of a band at 268 nm, together with its higher intensity relative to the intra-$^4F_8$ transition, shows an effective luminescence sensitization *via* the ligands excited states than the direct intra-$^4F_8$ excitation (Fig. 6).[21]

The luminescence emission spectrum of complex **3** was measured upon excitation at 268 nm (the maximum excitation wavelength). As shown in Fig. 6, the characteristic transitions of the Tb(III) ion from the emitting level ($^5D_4$) to the ground multiplet ($^7F_{6-3}$) are observed.[29] The $^5D_4 \rightarrow {}^7F_5$ transition is the strongest emission of the compound, corresponding to the emission of a bright green light. One intense emission band at 490 nm is ascribed to the $^5D_4 \rightarrow {}^7F_6$ transition of the Tb^{3+} ion and a sharp intense line emission at 546 nm corresponds to the $^5D_4 \rightarrow {}^7F_5$ transition of the Tb(III) ion, which gives intense green luminescence, while the two weak emission bands at 585 nm and 622 nm may be attributed to the $^5D_4 \rightarrow {}^7F_4$ and $^5D_4 \rightarrow {}^7F_3$ transitions, respectively.[30] The enhanced photoluminescence intensity observed for the Tb(III) complex may result from the efficient nonradiative deactivation mechanism of the excited states of the Tb(III) ion *via* O–H vibrations of the three coordinated water molecules to the metal ion.

Although the H_2PDH ligand triplet energy level lies above the emitter levels of the Tb(III) (resulting in an efficient sensitization) ion, the observed emission intensity is low due to the high number of vibrational oscillators, which contribute to a multiphonon deactivation of the excited states.[31] For the Tb(III) complex, even though some back transfer ($^5D_4 \rightarrow T_1$ energy transfer) processes can occur with an appreciable intensity, the ligand antenna effect is prominent and may be due to the proximity of the energy levels and the lower contribution of the vibrational deactivation (Fig. S4†).

The excitation spectra of complexes **4** and **4a** under the emission of 481 nm exhibit three main peaks, at 269 and 346 nm and a characteristic feature corresponding to the metal-centered transition at 367 nm ($^4M_{9/2} \leftarrow {}^6H_{15/2}$) for the Dy(III) derivatives.

The luminescence spectrum shows two apparent emission bands at 481 nm ($^4F_{9/2} \rightarrow {}^6H_{15/2}$) and 574 nm ($^4F_{9/2} \rightarrow {}^6H_{13/2}$) and a small band at 654 nm ($^4F_{9/2} \rightarrow {}^6H_{11/2}$) under the excitation of 269 nm (Fig. 7).[32]

Complex **4** exhibits the typical blue and yellow emission of Dy(III) for the $^4F_{9/2} \rightarrow {}^6H_n$ (n = 15/2, 13/2, 11/2) transitions, with a small intense band at 481 nm ($^4F_{9/2} \rightarrow {}^6H_{15/2}$).[26] It is obvious that the intensity of the blue emission, corresponding to the $^4F_{9/2} \rightarrow {}^6H_{15/2}$ transition, is a little stronger than that of the yellow one ($^4F_{9/2} \rightarrow {}^6H_{13/2}$). Further enhancement of the luminescence intensity to three fold was observed for complex **4a** (Fig. 7).

Based on the above results, it can be concluded that the luminescent lanthanide complexes are not only influenced by the energy level matching between the organic ligand and

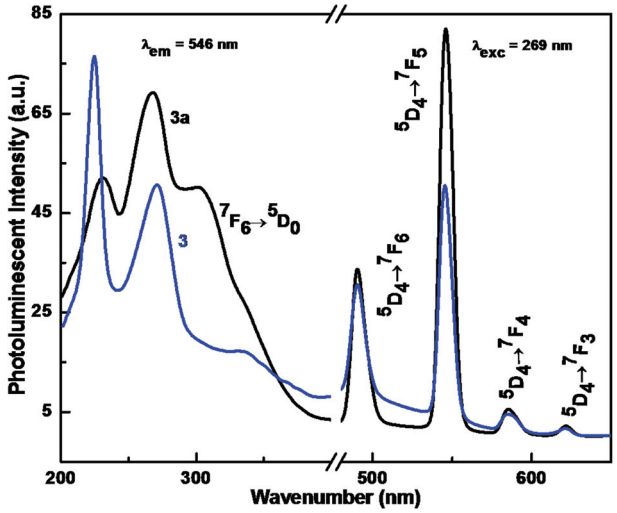

Fig. 6 Excitation and emission spectra of $Tb(HPDH)_3(H_2O)_3{\cdot}H_2O$ **3** (blue) and $Tb(HPDH)_3(H_2O)_3$ **3a** (black) at λ_{em} = 546 nm and λ_{exc} = 269 nm.

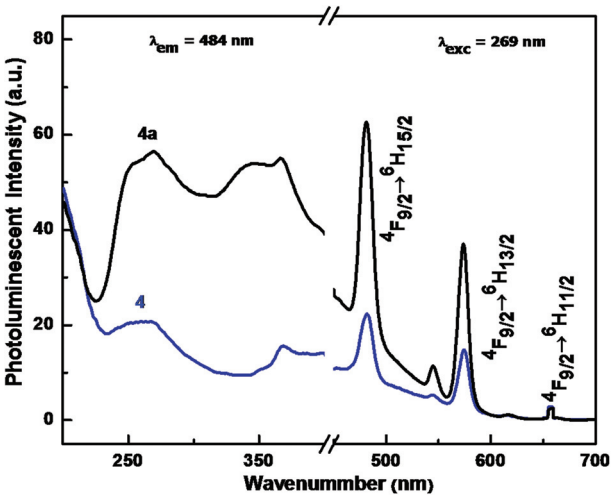

Fig. 7 Excitation and emission spectra of $Dy(HPDH)_3(H_2O)_3{\cdot}H_2O$ **5** (blue) and $Dy(HPDH)_3(H_2O)_3$ **4a** (black) at λ_{em} = 484 nm and λ_{exc} = 269 nm.

Ln(III) cation, but also by a weak vibronic coupling between the lanthanides and OH oscillators of coordinated water molecules, which normally provide a facile path for the radiationless deexcitation of Ln(III) ions.[33–35]

3.6. Thermal analysis

Thermogravimetric analysis (TGA) and differential thermogravimetric analysis (DTA) studies were performed in a nitrogen atmosphere at a heating rate of 10 °C min^{-1}. The complexes had similar TG curves (Fig. 8), and here complex **1** is used as a representative for discussion. The initial mass loss is ascribed to the loss of lattice water molecules, followed by the coordinated water molecules. The TGA-DTA curves for complex **1** reveals that the initial mass loss of 2.54%, between 85 and 163 °C, corresponds to the start of the departure of the lattice water molecules. The second major mass loss of 6.95% occurs between 163 and 295 °C, corresponding to three coordinated water molecules before 295 °C, the total mass loss is 9.49%, corresponding to the loss of four water molecules (calcd 10.1%). The decomposition of complex **1** begins above 295 °C, then complex **1** begins to decompose upon further heating and undergoes a rapid and significant weight loss of 69.1% in the temperature range of 295–937 °C, which corresponds to the destruction of the H_2PDH organic ligands (calcd 70.1%), and is consistent with the crystal structure analysis. The residue accounts for 19.1%, which is nearly in agreement with the calculated value of 19.8%, by assuming the final product is Sm_2O_3. The DTA curve exhibits three strong endothermic peaks at approximately 130, 246 and 834 °C, corresponding to the release of water molecules and decomposition of the organic fraction, respectively. Thermogravimetric analysis of compounds **1–4** reveals similar DT-TGA curves, which indicate three main steps of weight loss.

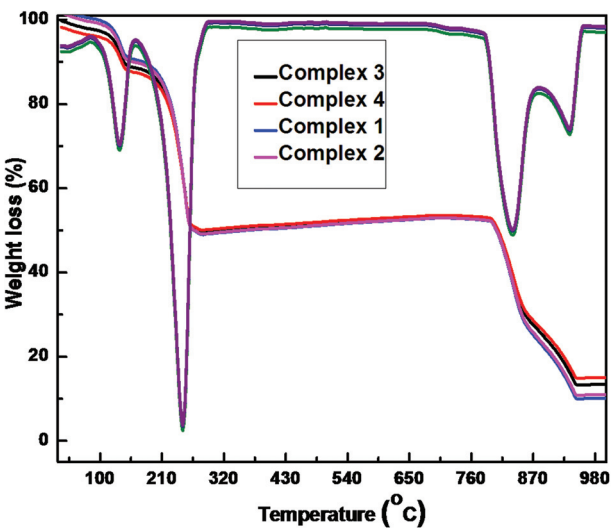

Fig. 8 Thermogravimetric analysis (TGA) and differential thermogravimetric analysis (DTA) curves in a nitrogen atmosphere at a heating rate of 10 °C min^{-1} for complexes **1–4**.

3.7. Potential of complexes for sensing small molecules

When a metal–organic complex interacts with polar solvents, intermolecular hydrogen bonds always form between the solvent molecules and lanthanide complexes.[36] These hydrogen bonds can change the solute and solvent electronic coupling, which can influence the luminescent properties of lanthanide complexes.[37] In order to understand the potential application of the title complexes for sensing solvents, the partially dehydrated Tb(III) complex **3a** was selected as a model for the study. The photoluminescent properties of complex **3a** were investigated in the solid-state and in nine pure solvents at room temperature. The photoluminescence spectra of the complex **3a**–solvent emulsions were measured after two days of aging and stirring vigorously before testing. The complex **3a**–solvent emulsions were prepared by introducing 2.00 mg of complex **3a** powder into 2.00 mL of each solvent (iso-propyl alcohol (IPA), ethanol (EtOH), methanol (MeOH), H_2O, acetonitrile (MeCN), DMF, acetone, $CHCl_3$, and THF) in glass tubes.

Under the same conditions their PL emission behavior was studied at an excitation wavelength of 270 nm, the PL emission spectra of all samples of complex **3a** shows two typical Tb(III) $^5D_4 \rightarrow {}^7F_n$ (n = 5, 4) transitions, among them the $^5D_4 \rightarrow {}^7F_5$ transition (546 nm) has the highest intensity, so the peak at 546 nm was selected as a reference for all further PL studies.

As shown in Fig. 9 and 10, the PL intensity is greatly dependent on the identity of the solvent molecule.[38] IPA has the strongest sensitizing effect and THF has a significant quenching influence on the luminescence intensity of complex **3a**, which almost disappeared when complex **3a** was immersed in pure THF, whereas others exhibit varying degrees of increasing sensitizing or quenching effects. Such solvent-dependent luminescence properties are very interesting and important for the selective sensing of IPA or THF solvent molecules.

In order to study the sensing effect in detail with respect to IPA, H_2O was selected as a reference solvent because its sensing effect appears in the middle of the nine different solvents. Different concentrations of IPA was added into a standard complex **3a**-emulsion in H_2O, while the concentration of

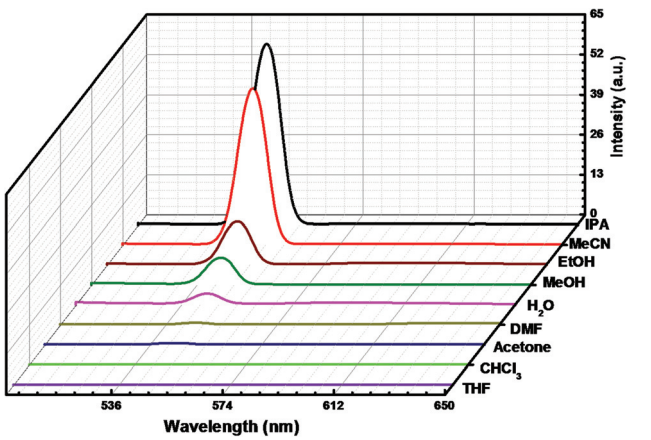

Fig. 9 The emission spectra of $Tb(HPDH)_3(H_2O)_3$ **3a**-emulsion in different solvents at room temperature, when excited at 270 nm.

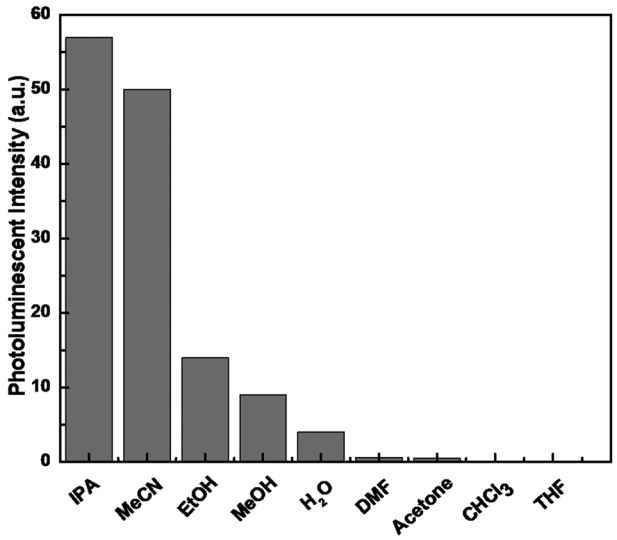

Fig. 10 Luminescence intensities of a $^5D_4 \rightarrow {}^7F_5$ transition of $Tb(HPDH)_3(H_2O)_3$ **3a**-emulsion in different solvents at room temperature, when excited at 270 nm.

Tb(III) was kept constant. Complex **3a** was dispersed in H_2O as a standard emulsion. As shown in Fig. 11, while the IPA concentration was gradually increased (5%, 25%, 50%, 75% and 100%), the PL intensity of the complex **3a**-emulsion gradually increased with the increasing concentration of IPA. The fluorescence enhancement was nearly proportional to the IPA concentration (inset in Fig. 11).

Additionally the reusability of complex **3a** was also studied by taking IPA, MeCN, EtOH and MeOH as examples. We explored the sensing ability of complex **3a** by filtering off the dispersed solution after use, washing several times with H_2O–EtOH and drying under vacuum at 423 K for 5 h. It is noteworthy that complex **3a** almost regains its initial fluorescence intensity (Fig. S5†), implying a high photostability of the material for a long time without any contamination.

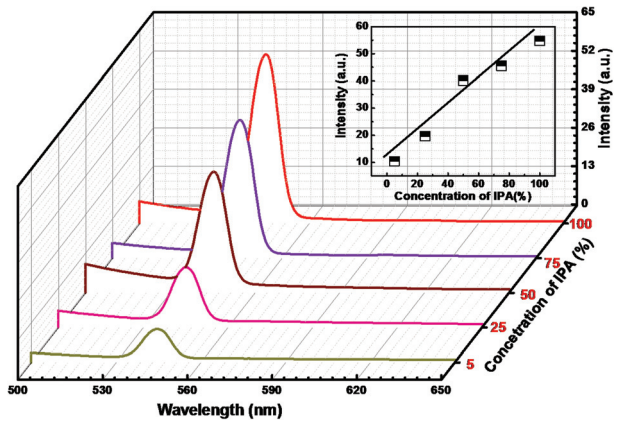

Fig. 11 The emission spectra of $Tb(HPDH)_3(H_2O)_3$ **3a**–IPA emulsion at different concentrations of IPA when excited at 270 nm. Inset shows the linear fluorescence enhancement *vs.* IPA concentration.

Interestingly, if the nine solvents are separated into two groups; protic solvents (IPA, EtOH, MeOH, H_2O) and the dipolar aprotic solvents (MeCN, acetone, $CHCl_3$, THF), and the photoluminescent intensities of these solvents were plotted against their dielectric constant and Reichardt values (Table 1), it could be observed that the PL intensity of complex **3a** decreases with the increase of the dielectric constant and normalized Dimroth–Reichardt E_T parameter (E_T^N) value for protic solvents, while the PL intensity increases with the increase of dielectric constant and for dipolar aprotic solvents (Fig. 12).[39–41]

Although the mechanism for the enhancing and quenching effects of small solvent molecules are still not clear, the binding interaction of the luminescent metal sites with guest solvent molecules definitely plays an important role. DMF has a different effect on the photoluminescence intensity due to its high coordination ability with Ln(III), which is known as a solvent effect. As shown in Fig. 2, the N and O donor sets of three H_2PDH ligands form a caved conformation, which is

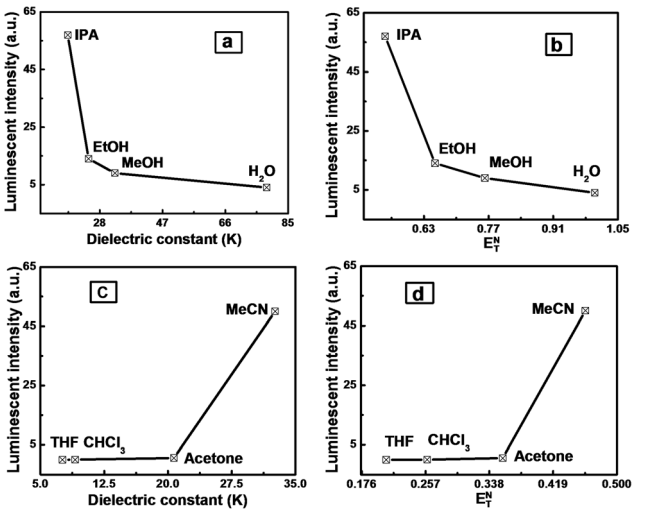

Fig. 12 Graphical representation of photoluminescence intensities of protic solvents with respect to the dielectric constant (a) and normalized Dimroth–Reichardt E_T parameter (E_T^N) values (b), and dipolar aprotic solvents with respect to the dielectric constant (c) and normalized Dimroth–Reichardt E_T parameter (E_T^N) values (d).

Table 1 Dielectric constant (K) and normalized Dimroth–Reichardt E_T parameter (E_T^N) values of different solvents[a]

Solvent	IPA	EtOH	MeOH	H_2O	MeCN	Acetone	$CHCl_3$	THF	DMF
K	18.3	24.6	32.6	78.54	37.5	20.7	4.81	7.6	36.7
E_T^N	0.546	0.654	0.762	1.0	0.460	0.355	0.259	0.207	0.386

[a] K = dielectric constant; E_T^N = normalized Dimroth–Reichardt E_T parameter.

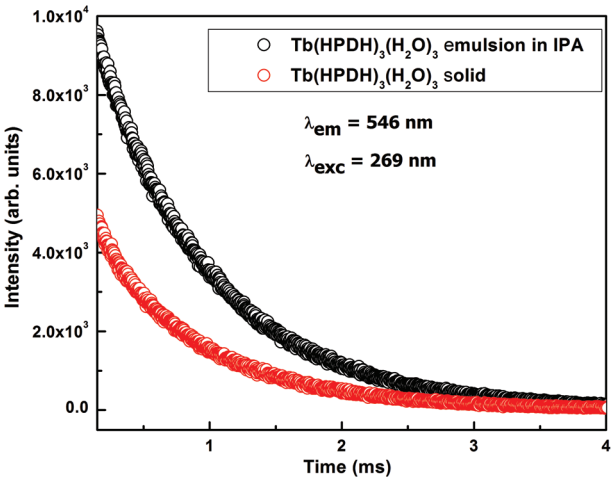

Fig. 13 Emission decay curves of the $^5D_4$ emitting state of Tb(HPDH)$_3$(H$_2$O)$_3$ (**3a**) in the solid state (red) and as an emulsion in IPA (black).

suitable for the coordination with Ln(III), however, this ajar cavity cannot prevent the solvent molecules from entering.[42] The three aqua ligands come to complete the coordination environment of Ln(III), however, they are easy to replace when other solvents are present. As a consequence, the entering solvent will consume either more or less energy than the ligand triple state energy transferring to the resonant energy level of the Ln(III).

It is believed that the coordinated H$_2$O molecules on the Tb(III) sites are gradually replaced by external solvent molecules, leading to their luminescence enhancement and/or diminishment, respectively. IPA was found to be an excellent sensitizer, while THF was a highly quenching solvent with a first order behavior on the photoluminescence intensity in this study (inset in Fig. 11).

3.8. Lifetime study

The $^5D_4$(Tb^{3+}) decay curves of Tb(HPDH)$_3$(H$_2$O)$_3$ (**3a**) in the solid state and its emulsion in IPA (**3a**-IPA) were monitored within the more intense line of the $^5D_4 \rightarrow {}^7F_5$ transition (546 nm) when excited at 269 nm. The emission decay curves (Fig. 13) were well fitted by a single-exponential function. The determined lifetime values of solid compound **3a** and **3a**-IPA emulsion are 0.81 ms and 0.97 ms, respectively. However, due to the extremely low intensity of the $^5D_4 \rightarrow {}^7F_5$ transition (λ_{em} 546 nm) of **3a** in THF, the emission decay curve of the **3a**-THF emulsion is not observable, indicating that the lifetime of the **3a**-THF emulsion is extremely small. This result is consistent with the results of the solvent sensing study.

4. Conclusion

Four mononuclear discrete lanthanide complexes Ln(HPDH)$_3$(H$_2$O)$_3$·H$_2$O [Ln = Sm(III) **1**, Eu(III) **2**, Tb(III) **3** and Dy(III) **4**], with a 3D supramolecular framework formed by hydrogen bonds and offset stacking (–H···π) interactions, were synthesized successfully. The compounds exhibited characteristic emissions of lanthanide cations in the solid states, indicating that the H$_2$PDH ligand is a promising candidate for various photonic applications in the future. The sensing study of small molecules by the partially dehydrated Tb(III) complex **3a** revealed that the nature of the solvent plays a key role in the enhancement or quenching of the photoluminescence of the complexes, and IPA was found to be an excellent sensitizer solvent while THF was a highly quenching solvent in this study and also both solvents show first order behavior towards the photoluminescence intensity. It was found that the photoluminescence intensity of complex **3a** decreases with the increase of the dielectric constant and normalized Dimroth–Reichardt E_T parameter (E_T^N) value for protic solvents, while the PL intensity increases with the increase of the dielectric constant and E_T^N for dipolar aprotic solvents. Complex **3a** excellently regained its initial photoluminescent intensity, revealing an interesting prospect for its long-term reusability. The results of this work may provide useful information about the design of stable, sensitive lanthanide complexes for the sensing of small guest molecules.

Acknowledgements

Financial support from the National Natural Science Foundation of China (no. 20975009) is greatly acknowledged.

Notes and references

1 (*a*) J. Zhou, W. Shi, N. Xu and P. Cheng, Highly selective luminescent sensing of fluoride and organic small-molecule pollutants based on novel lanthanide metal–organic frameworks, *Inorg. Chem.*, 2013, **52**, 8082–8090; (*b*) E. Y. Lee, S. Y. Jang and M. P. Suh, Multifunctionality and crystal dynamics of a highly stable, porous metal–organic framework [Zn$_4$O(NTB)$_2$], *J. Am. Chem. Soc.*, 2005, **127**, 6374–6381; (*c*) Y. Bai, G. He, Y. Zhao, C. Duan, D. Dang and Q. Meng, Porous material for absorption and luminescent detection of aromatic molecules in water, *Chem. Commun.*, 2006, 1530–1532; (*d*) B. Chen, Y. Yang, F. Zapata, G. Lin, G. Qian and E. B. Lobkovsky, Luminescent open metal sites within a metal–organic framework for sensing small molecules, *Adv. Mater.*, 2007, **19**, 1693–1696; (*e*) K. Binnemans, Lanthanide-based luminescent hybrid materials, *Chem. Rev.*, 2009, **109**, 4283–4374.

2 (*a*) W. Yang, J. Feng and H. Zhang, Facile and rapid fabrication of nanostructured lanthanide coordination polymers as selective luminescent probes in aqueous solution, *J. Mater. Chem.*, 2012, **22**, 6819–6823.

3 L. E. Kreno, K. Leong, O. K. Farha, M. Allendorf, R. P. V. Duyne and J. T. Hupp, Metalorganic framework materials as chemical sensors, *Chem. Rev.*, 2012, **112**, 1105–1125.

4 H.-L. Jiang, Y. Tatsu, Z.-H. Lu and Q. Xu, Non-, micro-, and mesoporous metal-organic framework isomers: reversible transformation, fluorescence sensing, and large molecule separation, *J. Am. Chem. Soc.*, 2010, **132**, 5586–5587.

5 (*a*) Y. Cui, Y. Yue, G. Qian and B. Chen, Luminescent functional metalorganic frameworks, *Chem. Rev.*, 2012, **112**, 1126–1162; (*b*) R. J. Kuppler, D. J. Timmons, Q.-R. Fang, J.-R. Li, T. A. Makal, M. D. Young, D. Yuan, D. Zhao, W. Zhuang and H.-C. Zhou, Potential applications of metal-organic frameworks, *Coord. Chem. Rev.*, 2009, **253**, 3042–3066.

6 G. Muller, Luminescent chiral lanthanide(III) complexes as potential molecular probes, *Dalton Trans.*, 2009, 9692–9707.

7 (*a*) D. Ma, W. Wang, Y. Li, J. Li, C. Daiguebonne, G. Calvez and O. Guillou, In situ 2,5-pyrazinedicarboxylate and oxalate ligands synthesis leading to a microporous europium–organic framework capable of selective sensing of small molecules, *CrystEngComm*, 2010, **12**, 4372–4377.

8 S. Nadella, P. M. Selvakumar, E. Suresh, P. S. Subramanian, M. Albrecht, M. Giese and R. Frolich, Lanthanide(III) complexes of bis-semicarbazone and bis-imine-substituted phenanthroline ligands: solid-state structures, photophysical properties, and anion sensing, *Chem.–Eur. J.*, 2012, **18**, 16784.

9 (*a*) A. D. Burrows, C.-W. Chan, M. M. Chowdhry, J. E. McGrady and D. M. P. Mingos, Multidimensional crystal engineering of bifunctional metal complexes containing complementary triple hydrogen bonds, *Chem. Soc. Rev.*, 1995, **24**, 329–339; (*b*) O. M. Yaghi, H. Li and T. L. Groy, Construction of porous solids from hydrogen-bonded metal complexes of 1,3,5-benzenetricarboxylic acid, *J. Am. Chem. Soc.*, 1996, **118**, 9096–9101; (*c*) W. A. Herrmann, N. W. Huber and O. Runte, Volatile metal alkoxides according to the concept of donor functionalization, *Angew. Chem., Int. Ed. Engl.*, 1995, **34**, 2187–2206; (*d*) G. R. Desiraju, Designer crystals: intermolecular interactions, network structures and supramolecular synthons, *Chem. Commun.*, 1997, 1475–1482; (*e*) G. M. Whitesides, E. E. Simanek, J. P. Mathias, C. T. Seto, D. N. Chin, M. Mammen and D. M. Gordan, Noncovalent synthesis: using physical-organic chemistry to make aggregates, *Acc. Chem. Res.*, 1995, **28**, 37–44.

10 A. M. Beatty, Hydrogen-bonded networks of coordination complexes, *CrystEngComm*, 2001, **51**, 1–13.

11 (*a*) G. M. Sheldrick, *SHELXTL V5.1, Software reference manual*, Bruker AXS, Inc, Madison, WI, 1997; (*b*) W. S. Sheldrick and M. Morr, *N*-Phosphonomethylglycin, *Acta Crystallogr., Sect. B: Struct. Crystallogr. Cryst. Chem.*, 1981, **37**, 733–734.

12 (*a*) G. M. Sheldrick, *SHELXTL-97, A program for crystal structure refinement*, University of Gottingen, Germany, 1997; (*b*) G. M. Sheldrick, *SHELXS97, Program for crystal structure solution*, University of Gottingen, Gottingen, Germany, 1997.

13 A. G. Talma, P. Jouin, J. G. de Vries, C. B. Troostwijk, G. H. W. Buning, J. K. Waninge, J. Visscher and R. M. Kellogg, Reductions of activated carbonyl compounds with chiral-bridged 1,4-dihydropyridines. An investigation of scope and structural effects, *J. Am. Chem. Soc.*, 1985, **107**, 3981–3997.

14 J. Jin, D. Wu, M. Jia, Y. Peng, J. Yu, Y. Wang and J. Xu, New 4,5-dichlorophthalhydrazidate-bridged chained coordination polymers, *J. Solid State Chem.*, 2011, **184**, 667–674.

15 (*a*) P. D. C. Dietzel, B. Panella, M. Hirscher, R. Blom and H. Fjellvag, Hydrogen adsorption in a nickel based coordination polymer with open metal sites in the cylindrical cavities of the desolvated framework, *Chem. Commun.*, 2006, 959–961; (*b*) F. Bonino, S. Chavan, J. G. Vitillo, E. Groppo, G. Agostini, C. Lamberti, P. D. C. Dietzel, C. Prestipino and S. Bordiga, Local structure of CPO-27-Ni metallorganic framework upon dehydration and coordination of NO, *Chem. Mater.*, 2008, **20**, 4957–4968.

16 A. J. Ivana, V. S. Zoran, S. D. Enis and M. N. Jovan, New hybrid properties of TiO_2 nanoparticles surface modified with catecholate type ligands, *Nanoscale Res. Lett.*, 2009, **5**, 81–88.

17 C. Emmeluth, B. L. Poad, C. D. Thompson and E. J. Bieske, Interactions between the chloride anion and aromatic molecules: infrared spectra of the $Cl–C_6H_5CH_3$, $Cl–C_6H_5NH_2$ and $Cl–C_6H_5OH$ complexes, *J. Phys. Chem. A*, 2007, **111**, 7322–7328.

18 A. Sengul and H. Arslan, Synthesis and characterization of novel polyamide and polyhydrazides based on the 6,6′-disubstituted-2,2′-bipyridine, *Turk. J. Chem.*, 2008, **32**, 355–364.

19 M. J. Rashkin and M. L. Waters, Unexpected substituent effects in offset π–π stacked interactions in water, *J. Am. Chem. Soc.*, 2002, **124**, 1860–1861.

20 E. D. la Rosa, L. A. Diaz-Torres, P. Salas and R. A. Rodrıguez, Visible light emission under UV and IR excitation of rare earth doped ZrO_2 nanophosphor, *Opt. Mater.*, 2005, **27**, 1320–1325.

21 P. Soares-Santos, L. Cunha-Silva, F. Paz, R. Ferreira, J. Rocha, L. Carlos and H. Nogueira, Photoluminescent lanthanide-organic bilayer networks with 2,3-pyrazinedicarboxylate and oxalate, *Inorg. Chem.*, 2010, **49**, 3428–3440.

22 (*a*) Y.-F. Yuan, T. Cardinaels, K. Lunstroot, K. Van Hecke, L. Van Meervelt, C. Gorller-Walrand, K. Binnemans and P. Nockemann, Rare-earth complexes of ferrocene-containing ligands: visible-light excitable luminescent materials, *Inorg. Chem.*, 2007, **46**, 5302–5309; (*b*) D. Weng, X. Zheng, X. Chen, L. Li and L. Jin, Synthesis, upconversion luminescence and magnetic properties of new lanthanide–organic frameworks with (43)2(46, 66, 83) topology, *Eur. J. Inorg. Chem.*, 2007, 3410–3415.

23 B. Francis, D. B. Ambili Raj and M. L. Reddy, Highly efficient luminescent hybrid materials covalently linking with europium(III) complexes *via* a novel fluorinated β-diketonate ligand: synthesis, characterization and photophysical properties, *Dalton Trans.*, 2010, **39**, 8084–8092.

24 J. H. Forsberg, Complexes of lanthanide(III) ions with nitrogen donor ligands, *Coord. Chem. Rev.*, 1973, **10**, 195–226.

25 A. F. Kirby, D. Foster and F. S. Richardson, Comparison of $^7F_J \leftarrow {}^5D_0$ emission spectra for Eu(III) in crystalline environments of octahedral, near-octahedral, and trigonal symmetry, *Chem. Phys. Lett.*, 1983, **95**, 507–512.

26 G. R. Choppin and D. R. Peterman, Applications of lanthanide luminescence spectroscopy to solution studies of coordination chemistry, *Coord. Chem. Rev.*, 1998, **174**, 283–293.

27 Y. Sun, X. Yan, F. Ding, E. Gao, W. Zhang and F. Verpoort, A novel 3D 4d–4f heterometallic coordination polymer: Synthesis, crystal structure and luminescence, *Inorg. Chem. Commun.*, 2008, **11**, 1117–1120.

28 Z. Zhang, J. Yuan, X. Wang, D. Xiong, H. Chen, J. Zhao, Y. Fu, Z. Qi, G. Zhang and C. Shi, Luminescence properties of $CaZr(PO_4)_2$:RE (RE = Eu^{3+}, Tb^{3+}, Tm^{3+}) under X-ray and VUV–UV excitation, *J. Phys. D: Appl. Phys.*, 2007, **40**, 1910–1914.

29 L. Zhang, S. Xu, Y. Zhou, X. Zheng, C. Yu, Z. Shi, S. Hassan and C. Chen, Two isomorphous 3-D lanthanide oxalatophosphonate frameworks based on glyphosate: syntheses, crystal structures, and luminescence properties, *CrystEngComm*, 2011, **13**, 6511–6519.

30 U. Caldino, A. Speghini and M. Bettinelli, Optical spectroscopy of zinc metaphosphate glasses activated by Ce^{3+} and Tb^{3+} ions, *J. Phys.: Condens. Matter*, 2006, **18**, 3499–3508.

31 J. C. G. Bunzli and G. R. Choppin, *Lanthanide probes in life, chemical and earth sciences*, Elsevier, Amsterdam, Netherlands, 1989.

32 H. Xiumei, L. Jun, L. Zhe, Q. Xiwei, L. Mingya and W. Xiaoqiang, Photoluminescent properties of $Ca_2Gd_8(SiO_4)_6O_2$: Dy^{3+} phosphor films prepared by sol-gel process, *J. Rare Earths*, 2008, **26**, 904–906.

33 F. J. Steemers, W. Verboom, D. N. Reinhoudt, E. B. Van der Tol and J. W. Verhoeven, New sensitizer-modified calix[4]arenes enabling near-UV excitation of complexed luminescent lanthanide ions, *J. Am. Chem. Soc.*, 1995, **117**, 9408–9414.

34 M. Latva, H. Takalo, V.-M. Mukkala, C. Matachescu, J. C. Rodriguez-Ubis and J. J. Kankare, Correlation between the lowest triplet state energy level of the ligand and lanthanide(III) luminescence quantum yield, *J. Lumin.*, 1997, **75**, 149–169.

35 M. V. Lucky, S. Sivakumar, M. L. P. Reddy, A. K. Paul and S. Natarajan, Lanthanide luminescent coordination polymer constructed from unsymmetrical dinuclear building blocks based on 4-((1H-benzo[*d*]imidazol-1-yl)methyl)-benzoic acid, *Cryst. Growth Des.*, 2011, **11**, 857–864.

36 (*a*) S. Zhang, Z. Wang, H. Zhang, Y. Cao, Y. Sun, Y. Chen, C. Huang and X. Yu, Self-assembly of two fluorescent supramolecular frameworks constructed from unsymmetrical benzene tricarboxylate and bipyridine, *Inorg. Chim. Acta*, 2007, **360**, 2704–2710; (*b*) F. Liu, H. Hao, C. Sun, X. Lin, H. Chen, R. Huang and L. Zheng, Syntheses, structures, and photoluminescences of four Cd(II) coordination architectures based on 1-(4-pyridylmethyl)-2-methylimidazole and aromatic carboxylates: from one-dimensional chain to three-dimensional coordination architecture, *Cryst. Growth Des.*, 2012, **12**, 2004–2012.

37 (*a*) G. Li, G. Zhao, K. Han and Y. Liu, TD-DFT study on the sensing mechanism of a fluorescent chemosensor for fluoride: excited-state proton transfer, *J. Comput. Chem.*, 2010, **31**, 1759–1765; (*b*) G. Zhao and K. Han, Hydrogen bonding in the electronic excited state, *Acc. Chem. Res.*, 2012, **45**, 404–413.

38 D. Ma, W. Wang, Y. Li, J. Li, C. Daiguebonne, G. Calvez and O. Guillou, *In situ* 2,5-pyrazinedicarboxylate and oxalate ligands synthesis leading to a microporous europium–organic framework capable of selective sensing of small molecules, *CrystEngComm*, 2010, **12**, 4372–4377.

39 J. A. Riddick, W. B. Bunger and T. K. Sakano, *Organic solvents: physical properties and methods of purification*, John Wiley and Sons, New York, 4th edn, 1986.

40 R. Diaz-Torres and S. Alvarez, Coordinating ability of anions and solvents towards transition metals and lanthanides, *Dalton Trans.*, 2011, **40**, 10742–10750.

41 R. Christian, Solvatochromic dyes as solvent polarity indicators, *Chem. Rev.*, 1994, **94**, 2319–2358.

42 (*a*) M. Kanesato, K. Nagahara, K. Igarashi, K. Sato, Y. Kikkawa and M. Goto, Synthesis, characterization and emission properties of yttrium(III) and europium(III) complexes of a tripodal heptadentate Schiff-base ligand $N[CH_2CH_2N = CH(2\text{-}OH\text{-}3\text{-}MeC_6H_3)]_3$, *Inorg. Chim. Acta*, 2011, **367**, 225–229; (*b*) R. Gheorghe, M. Andruh, A. Muller and M. Schmidtmann, Heterobinuclear complexes as building blocks in designing extended structures, *Inorg. Chem.*, 2002, **41**, 5314–5316; (*c*) G. Rajaraman, F. Totti, A. Bencini, A. Caneschi, R. Sessoli and D. Gatteschi, Density functional studies on the exchange interaction of a dinuclear Gd(III)-Cu(II) complex: method assessment, magnetic coupling mechanism and magneto-structural correlations, *Dalton Trans.*, 2009, 3153–3161.

